METEOROLOGICAL APPLICATIONS
Meteorol. Appl. **19**: 54–70 (2012)
Published online 19 April 2011 in Wiley Online Library
(wileyonlinelibrary.com) DOI: 10.1002/met.257

RMetS
Royal Meteorological Society

Temporal extension of meteorological records for hydrological modelling of Lake Chad Basin (Africa) using satellite rainfall data and reanalysis datasets

Satish Bastola[a]* and Delclaux François[b]
[a] *ICARUS, National University of Ireland, Maynooth Co., Kildare, Ireland*
[b] *IRD, UMR Hydrosciences Montpellier (CNRS/IRD/UMI/UMII), MSE, F-34095 Montpellier, France*

ABSTRACT: The inability to estimate reliable meteorological data for the hydrological modelling of the Lake Chad Basin (LCB) over the present decade hinders the use and evaluation of a wide range of hydrological information that can be extracted from satellite altimetry, gravitometry, and imagery. This is mainly due to the sparse distribution of gauging stations and difficulty in data assessment. Therefore, two key chronological records of rainfall and potential evapotranspiration (PET) were constructed for flow simulation modelling in the LCB. Rainfall estimates were extracted from two satellite-based precipitation products for the period 1998–2007 and combined with available chronological rainfall data. Similarly, PET records were derived over the period 1948–2007 using the meteorological variables extracted from reanalysis datasets, and the Hargreaves method. Subsequently, they were evaluated, first by pairwise comparison against available gridded datasets, and second by analyzing the error propagated through a distributed hydrological model.

The satellite products strongly agree with the rain gauges. Compared to gridded rainfall estimates from the Climate Research Unit (CRU), satellite products tend to underestimate the values in the southern and eastern mountainous regions of the LCB and overestimate them within the central part of the LCB. Furthermore, flows simulated using the satellite products are in closer agreement with observed discharges than those modelled using CRU data. Concerning PET, the estimates from the Hargreaves method were compared with two gridded PET datasets: Penman PET data derived using climate data of the CRU, and climatological PET data from the Food and Agriculture Organization.

KEY WORDS hydrological model; potential evapotranspiration; satellite precipitation products; reanalysis meteorological dataset

Received 22 June 2010; Revised 14 January 2011; Accepted 31 January 2011

1. Introduction

Hydrological data have always played a fundamental role in planning and formulating sound policies for the sustainable management of water resources. This role has become even more crucial in today's environment, where competition among water users is increasing and hydrological networks are found to be either declining or inadequate in reproducing spatial and temporal hydrological data. Consequently, hydrological models are often used to generate hydrological data in regions where no previous observations have been made. Due to the randomness in nature and the lack of complete knowledge regarding hydrological systems, uncertainty is an unavoidable element in any hydrological modelling study (Gupta *et al*., 2003). The use of multiple catchment response data can help in reducing the predictive uncertainty of hydrological models (Kuczera and Mroczkowski, 1998). More recently, a wide range of studies have focused on the extraction of terrestrial information from satellite imagery, including spatial and temporal information of the Earth's water storage using gravity recovery (Güntner *et al*., 2007), the spatial and temporal surface-water bodies derived from optical remote sensing data (Haas *et al*., 2009) and time series of water level variations in lakes and reservoirs derived from TOPEX-POSEIDON/ENVISAT using satellite altimetry (Coe and Birkett, 2004; Frappart *et al*., 2006). These datasets have the potential to characterize the spatial-temporal variations in terrestrial information better and provide additional data that can help reduce the predictive uncertainty of hydrological models. A wide range of satellite-derived data on terrestrial information is available for the Lake Chad Basin (LCB). However, the unavailability of meteorological records within the LCB, especially after the 1990s, is a major constraint for the successful application of hydrological models and subsequent evaluation of these datasets. Furthermore, the accuracy of hydrological model predictions depends on the accuracy of rainfall

* Correspondence to: S. Bastola, ICARUS, National University of Ireland Maynooth Co. Kildare, Ireland.
E-mail: Satish.Bastola@nuim.ie; delclaux@msem.univ-montp2.fr

measurements (Paturel *et al*., 1995; Nandakumar and Mein, 1997) and also the method employed for the estimation of potential evaporation (e.g. Vörösmarty *et al*., 1998; Andreassian *et al*., 2004).

Global gridded rainfall and potential evaporation have found applications in data sparse regions. The Global Precipitation Climatology Center (GPCC) Version 3 is one such dataset that is available for the 1951–2004 period with a spatial resolution of 0.5° (Rudolf and Schneider, 2004). The CRUTS2.1 (referred to as CRU hereafter) (Mitchell and Jones, 2005) is another such dataset that provides the monthly precipitation for each 0.5° cell and has been used in many global studies (e.g. Döll *et al*., 2003). The estimate from CRUTS2.1, which has been used in modelling the LCB on a number of instances (e.g. Coe and Foley, 2001; Delclaux *et al*., 2008), is only available for data prior to 2002. Recently, the rainfall estimates from CRU are becoming less reliable within the LCB: the number of gauging stations has sharply declined due to financial constraints. In this context, monitoring rainfall from satellite imagery is an attractive alternative in the LCB region.

Several studies of the satellite estimated rainfall in Africa were published in recent years (e.g. McCollum *et al*., 2000; Adeyewa and Nakamura, 2003; Ali *et al*., 2005; Dinku *et al*., 2008). McCollum *et al*. (2000) report that the Global Precipitation Climatology Project (GPCP) satellite estimates are approximately twice the magnitude of estimates produced from the rain gauges used by the GPCP in central equatorial Africa. The authors reasoned that the abundance of aerosol and a higher cloud base were possible explanations for the discrepancies. Over the land area of Africa, Adeyewa and Nakamura (2003) observed significant seasonally and regionally dependent biases in the estimates from both the TRMM3B43 and TRMM Precipitation Radar (TRMM PR) and Tropical Rainfall Measuring Mission (TRMM). Moreover, their study revealed that TRMM3B43 is in closer agreement with rain gauge data in the major climatic regions of Africa as compared to estimates from TRMM PR. In a similar study that used data with different spatial resolutions, Ali *et al*. (2005) investigated the accuracy of various global rainfall products in the Sahel region and found that the estimates from the merged analysis of precipitation from the Climate Prediction Center (CPC) is the best overall product, followed by GPCC, GPCP, and the Geostationary Operational Environmental Satellite Precipitation Index (GPI), which had the largest errors associated with it. Dinku *et al*. (2008) evaluated five global gridded monthly precipitation products (variants of GPCC, CPC and CRU) using a gauge network of 150 stations over a complex mountainous terrain located over the Ethiopian highlands. They found a very good agreement between global products and the reference data at different spatial scales (e.g. 2.5°, 1.0° and 0.5°).

Most of these studies focused either on the evaluation of satellite rainfall algorithms or on the accuracy of precipitation products in their specified region. However, comparisons of estimates from satellite in Central and Western Africa, where slight changes in precipitation result in dramatic changes in the runoff response due to the fact that the runoff generation is highly nonlinear, is rare. Since the LCB extends across different climatic zones, the impact of error in rainfall estimates will have varying impact in the runoff. Therefore, it is essential to evaluate these products at the basin scale from a hydrological point of view.

Within the LCB, the instruments and practices used to measure the evapotranspiration vary considerably from country to country and the quality and quantity of data, which are required for the evaluation of empirical models, are not consistent among the regions. Furthermore, for the region within the LCB, climatological data can usually be found in the literature, but monthly or annual time series of evaporation data are scarce (Shahin, 2002). Therefore, estimations of reliable potential evapotranspiration (referred to as PET hereafter) for hydrological simulation models are equally important, since it is the primary input in such a model.

Over the years, many relationships for the estimation of PET from standard meteorological variables have been developed (e.g. Penman, 1948; Makkink, 1957; Hargreaves and Samani, 1985). The details of these methods can be found in Singh and Xu (1997). Kay and Davies (2008) compared the performance of the Penman–Monteith method and a simple temperature-based method forced with data from a climate model, with a gridded reference evapotranspiration dataset of the Met Office Rainfall and Evaporation Calculation System (MORECS) over Britain. They observed that simple empirical models reproduced the MORECS dataset better than the Penman–Monteith method. They suggested reasons for such an outcome, which included the differences in the reliability of the variables simulated by climate models. Such reliability problems were reduced when only temperature data were used. Similarly, Oudin *et al*. (2005) used 27 different evapotranspiration models on 308 catchments located in Australia, France and the United States. They showed that the model based on temperature and radiation tends to provide better streamflow simulation than the Penman approach. Although Penman's method has been widely used because of its strong theoretical foundation and more general applicability than other methods, the dependency of Penman's method on weather data, which are not readily available in most of the stations, limits its application in data sparse regions such as Africa. Consequently, empirical models are widely preferred in data sparse regions.

Therefore, this study is a preliminary attempt to extend the meteorological records using satellite-derived rainfall products and potential evapotranspiration estimated using reanalysis data for the simulation modelling of the LCB. Section 2 provides a description of the study basin. In Section 3, the reference and satellite-based precipitation datasets are described together with the methodology. Section 4 presents the results and discussion. Finally, conclusions are drawn.

2. Study area

The Lake Chad Basin (2.4 million km^2) lies between 5 and 26 °N, and 7 and 24 °E in Central Africa. It expands across the Saharan, Sahelian, and Sudanese zones and spreads over seven countries (Figure 1). It is bounded by the Tibesti, Hoggar and Aïr mountains to the north/northwest, the Ennedi and Ouaddai mountains to the east, and the Adamawa mountain and Joss plateau to the south. The theoretical hydrological basin can be divided into the southern part (hydrologically active) and the northern part (hydrologically inactive). Under present climatic conditions, the lake receives water mainly from the Chari-Logone river system. The Chari is the longest river in the basin with a catchment area of 0.6 m km^2, which is a quarter of the total area of the basin. It has an average annual runoff of 40×10^9 m^3, producing 90% of the surface discharge into the lake, whereas the remaining 10% is supplied by minor tributaries such as the Komadougou River. The principal lake water losses are first due to evaporation, more than 2 m year^{-1}, and second due to infiltration. A comprehensive review of the hydrological characteristics of the LCB can be found in Roche (1980), Gac (1980) and Olivry *et al.* (1996). The River Chari flows from the Central African Republic through Chad into Lake Chad, following the Cameroon border downstream of N'Djamena, where it joins the River Logone. The River Logone is a major tributary of the Chari-Logone river system. The Logone's sources are located in the Western Central African Republic, Northern Cameroon and Southern Chad. Consequently, and due to the south-north extent of the basin, the lake water balance mainly depends on humid areas for water inputs from tributaries and semi-arid zones for water losses due to lake evaporation.

Another important feature of the basin concerns depressions and floodplains. As the basin is predominately flat with an overall median slope of 1.3% (Le Coz *et al.*, 2009), it houses extensive floodplains and many local depressions. The potential water areas and depression surfaces calculated from the 5′ Digital Elevation Model (DEM) and aggregated from 3″ SRTM DEM are nearly 10% of the Chari-Logone basin area. These potential water storage areas and floodplains play a pivotal role in the regional water balance as they provide more opportunity for evaporation. The evaporation volume over the basin can reach 25 km^3 year^{-1} (Gac, 1980).

3. Data and methods

3.1. Reference gauged rainfall and meteorological data

The reference rain gauge and hydrometeorological data for the LCB region are obtained from the Système d'Information Environnementales sur les Ressources en Eau et Leur Modelisation (SIEREM) (Boyer *et al.*, 2006). The hydrometeorological data stored by SIEREM have been updated more recently by HydroSciences Montpellier. The estimates of 26 gauging stations for which records are mostly available during the satellite data period were extracted from the SIEREM database. The location of these stations is shown in Figure 2. Though the station data from SIEREM cover a large part of Central and Western Africa (Mahé *et al.*, 2001), the gauging stations selected in this study are mostly located in the southwestern part of the LCB region. Moreover, the gauging stations can be grouped into three zones as suggested by Deichmann and Eklundh (1991): (1) arid (0.05 < rainfall/PET < 0.2), (2) semi-arid (0.2 < rainfall/PET < 0.5), and (3) humid zone (rainfall/PET > 0.5). Among the 26 stations, 6 are located in humid zone, 10 in the semi-arid zone and 10 in the arid zone (Figure 2). Furthermore, temperature, solar radiation, and measured evapotranspiration data from the Bol Matafo station were collected in order to model the potential evapotranspiration.

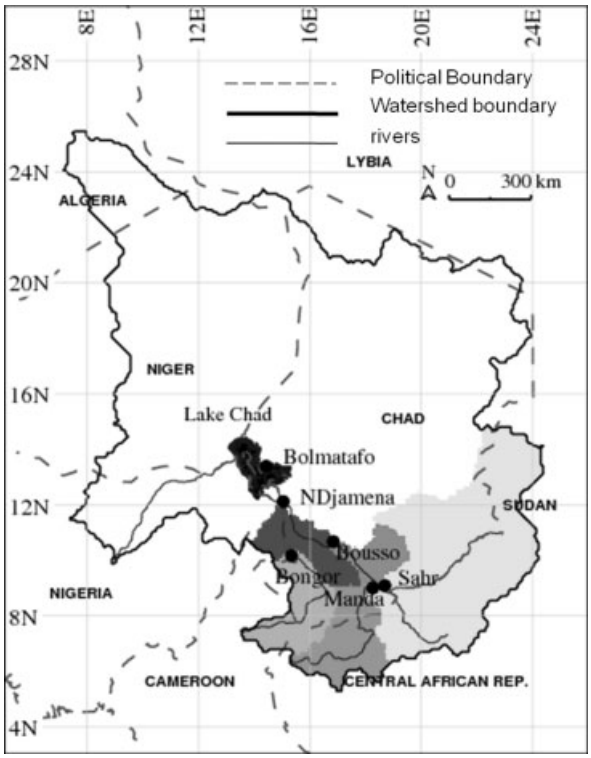

Figure 1. Geographic political location of Lake Chad Basin. The hydrologically active part of the basin is mainly drained by Chari-Logone river system in the southern part. Major sub-basins are Sahr, Manda, Bongor, and Bousso.

3.2. Gridded rainfall and meteorological data

Four gridded precipitation datasets, TRMM3B43, GPCP 1Degree Day, African Rainfall Estimation Algorithm version 2 (RFE2.0) and CRUTS2.1, were considered for this study. These products cover our target region and are available at high spatial resolutions. Figure 3 shows the spatial and temporal coverage of the gridded rainfall datasets.

GPCP1DD is a satellite gauge blend product of GPCC that was developed by Huffman *et al.* (2001). It is presently the only satellite-based precipitation product that is available at a daily time step and covers the

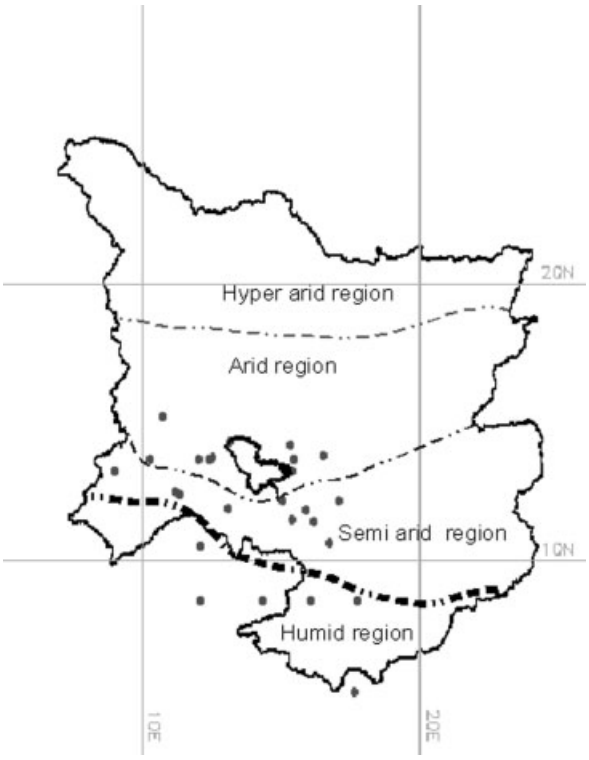

Figure 2. Location of rainfall gauging stations within various climatic regions of Lake Chad Basin.

entire globe. The satellite-based precipitation estimates are then scaled to match monthly GPCP Version 2 satellite gauge precipitation estimates (Adler *et al*., 2003). The GPCP1DD data were taken from Huffman and Bolvin (2009).

The TRMM3B43 is a satellite gauge blend product, which uses the 3-hourly merged high-quality/IR estimates (3B-42RT), and either the monthly-accumulated Climate Assessment and Monitoring System, or the Global Precipitation Climatology Center (GPCC) rain gauge analysis. The algorithm is based on the techniques by Huffman *et al*. (1997). The output of the TRMM3B43 is the monthly rainfall for $0.25^\circ \times 0.25^\circ$ grid boxes and covers an area extending from 50 °N to 50 °S. The TRMM3B43 data were taken from GES DISC (2010).

The African Rainfall Estimation Algorithm version 2.0 (RFE2.0) is the rainfall product from the operational CPC Africa rainfall algorithm. In REF2.0, information from three different satellites is first combined linearly using predetermined weighting coefficients. Subsequently they are merged with station data to determine the final rainfall product. The output of this product is the daily precipitation estimates at $0.1^\circ \times 0.1^\circ$ spatial scales and extends from 40 °S to 40 °N and 20 °W to 55 °E. These data were taken from CPC (2006). Another precipitation dataset that is widely used in global studies is obtained from the CRU. This database consists of monthly climate observations constructed at a spatial resolution of $0.5^\circ \times 0.5^\circ$ from meteorological stations. The climate grids are constructed for nine climate variables over the period of 1901–2002. Despite the data collection efforts, the CRU data in many regions still represent only a sub-set of the potentially available stations. Figure 4, which is a plot of the temporal evolution of gauging stations within the LCB region, shows that the number of gauging stations used in deriving CRU precipitation estimates over the LCB region has markedly decreased, from nearly 150 to only 75 stations, since 1990.

The time series of solar radiation and temperature data that are required for modelling evapotranspiration data using empirical models are extracted from the National Center for Atmospheric Research (NCEP/NCAR) for the period of 1948–2007. These data, originally at a resolution of $2.5^\circ \times 2.5^\circ$, were re-gridded to conform to the resolution of the $0.5^\circ \times 0.5^\circ$ using bilinear interpolation.

In order to evaluate the estimated PET, two reference gridded PET datasets were extracted for the LCB region. The time series of PET that estimates rainfall for the

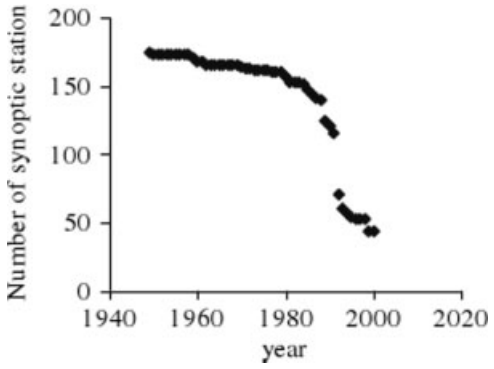

Figure 4. Evolution of gauging stations, within the Lake Chad Basin, used to derive CRUTS2.1 precipitation dataset.

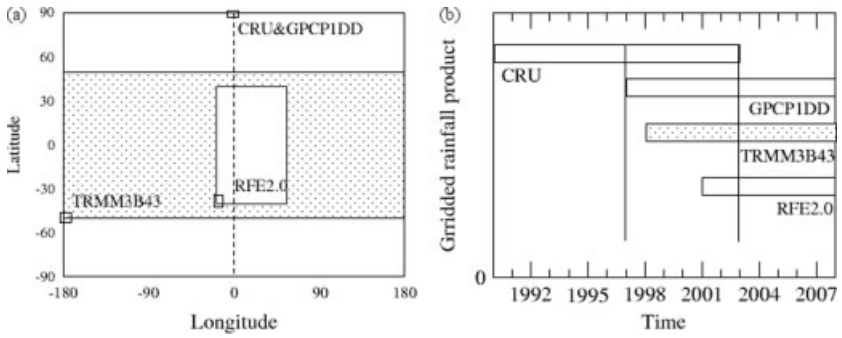

Figure 3. Characteristics of gridded precipitation datasets; (a) spatial coverage, (b) temporal coverage.

LCB (referred to as the LCB_PET hereafter) uses the Penman formula (Peixoto and Oort, 1992) forced with the CRU climate data. These data are available at $0.5^\circ \times 0.5^\circ$ for the LCB region and can be downloaded from Sage (2010). These data have been widely used in the past for flow simulation modelling of the LCB (e.g. Coe and Foley, 2001; Delclaux *et al*., 2008). Previously they were used as control data for the evaluation of estimated PET.

3.3. Construction of rainfall data scenarios

Satellite rainfall datasets are generally available for relatively shorter periods of time than generally required for hydrological modelling. Moreover, they include errors such that a correction is needed to make them consistent with existing data so that the data are reliable, available for longer time period, and able to be used for model calibration. Within the LCB, the only gridded precipitation product that is currently available at a fine scale that extends for a long period of time is the CRU dataset. Therefore, in this study, the following five rainfall datasets (1901–2007) were constructed using satellite precipitation products and CRU (Figure 5): (1) concatenating CRU and GPCP (referred as GPCP), (2) concatenating CRU and TRMM (referred as TRMM), (3) concatenating CRU with the average of the estimates from GPCP and TRMM (referred as Ave(GPCP, TRMM)), (4) concatenating CRU and estimates inferred from the linear relationship between GPCP and CRU over an overlapping period (referred as CRU_GPCP), and, (5) concatenating CRU and estimates inferred from the linear relationship between TRMM and CRU over an overlapping period (referred as CRU_TRMM). Since the CRU, GPCP and TRMM data are available at different spatial scales, the satellite precipitation products were suitably regridded to conform to the spatial resolution ($0.5^\circ \times 0.5^\circ$) of CRU. The TRMM, which is available at 0.25°, was regridded at 0.5° using spatial averaging, whereas bilinear interpolation was used to regrid GPCP from 1° to 0.5°.

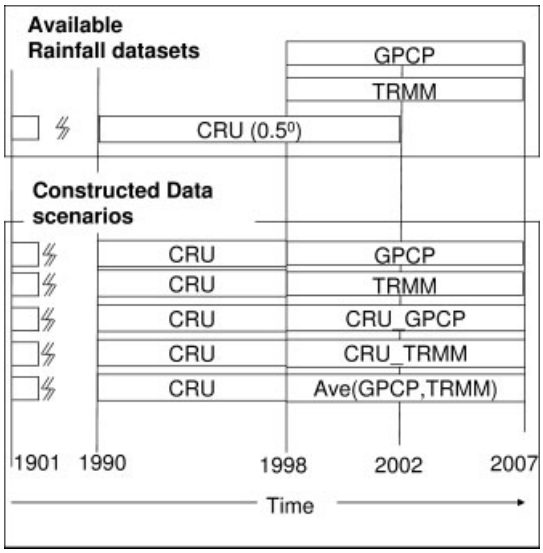

Figure 5. Schematic of rainfall data scenarios based on satellite precipitation products. Ave(GPCP, TRMM) is the average of the two satellite products, CRU_GPCP (respectively CRU_TRMM) is derived from the linear relationship between CRU and GPCP (respectively TRMM) over the common period.

3.4. Estimation of potential evapotranspiration

Owing to the simplicity of empirical methods and their potential to reproduce results comparable to physically based models (Abtew, 2001), a generalized form of the Hargreaves method (Xu and Singh, 2000 for detail) is considered in this study. It is an empirical method that uses solar radiation and temperature (Equation (1)) to compute daily/monthly PET:

$$PET = a(T + b) \times \frac{Rs}{\lambda} \tag{1}$$

where R_s is the incoming solar radiation (W m^{-2}), T is the air temperature (°C), a and b are constants, λ is the latent heat of vapourization expressed in MJ Kg^{-1}, and PET is in mm $month^{-1}$. The estimation of PET from Equation (1) involves specifying the value of constants a and b, which are the time series of solar radiation and temperature, respectively.

Since the constants for the model as given by Xu and Singh (2000) (referred to as constants from the literature hereafter) may only be reliable in the areas and over the periods for which they were determined, the a and b constants in Equation (1) can be calibrated for the LCB region using observed data. Calibration of these constants was achieved with monthly evapotranspiration data from the Thornthwaite-type evapotranspirometer installed at the Bol Matafo station (1965–1977). Moreover, due to the unavailability of reliable solar radiation data, meteorological data, i.e. solar radiation and air temperature extracted from NCEP/NCAR, were used. The period 1973–1977 was used to calibrate the constants and the period 1965–1972 was used for the validation step. The values of these constants were adjusted so that the differences between measured and model estimated PET values are minimal.

3.5. Methods of evaluation

3.5.1. Pairwise comparison

Pairwise comparisons of satellite rainfall products are made with: (1) a network of 26 gauging stations from SIEREM, and (2) the CRU rainfall dataset. Several objective criteria were used to substantiate this comparison, including bias (Equation (2)), RMSE (Equation (3)), and Nash-Sutcliffe Efficiency (NSE) (Equation (4)):

$$Bias = \frac{1}{n}\sum_{i=1}^{n}(e_i - m_i) \tag{2}$$

$$RMSE = \sqrt{\frac{\sum_{i=1}^{n}(e_i - m_i)^2}{n}} \quad (3)$$

$$NSE = 1 - \frac{\sum_{i=1}^{N}(e_i - m_I)^2}{\sum_{i=1}^{N}(m_i - \overline{m})^2} \quad (4)$$

where m is the measured and/or control value, e is the estimated quantity, $\overline{m}^2$ is the average value of measured and/or control value, and n is the number of available data points.

While satellite estimates represent the pixel average value at a given instance in time, rain gauges measure rainfall as a time integral of rain at a particular location. However, the numbers of gauging stations within the grid box ($0.5^\circ \times 0.5^\circ$) covering the satellite period are extremely low within the LCB region and the number of missing values at available stations is large. In addition, the timely collection of rainfall data from stations within the LCB region is difficult, as the LCB is shared by seven different countries. Therefore, at this stage of the study, no attempt has been made to construct a rainfall grid from the gauge data. Instead, the satellite data were compared with the rainfall from gauging stations and from the CRU.

Concerning the PET estimates, the pairwise comparisons were made between the Hargreaves-estimated PET and two reference datasets: (1) global map of climatological reference evapotranspiration from FAO (2004), and, (2) the time series of the PET data, i.e. the LCB_PET. To conform with the spatial scale of the output from the Hargreaves method, the climatological data of the FAO available at $10' \times 10'$ were re-gridded at a scale of $0.5^\circ \times 0.5^\circ$ using the spatial averaging method. Pairwise comparisons between the Hargreaves PET and the control PET were conducted using the same objective criteria that were defined for the evaluation of precipitation datasets.

3.5.2. *Hydrological modelling*

The schematic for the evaluation of meteorological records using the hydrological model is shown in Figure 6. In this methodology, the test datasets are evaluated by analyzing: (1) discrepancies between the outputs of the model forced with the test data and control data (this method being referred to as model propagated error hereafter), and, (2) discrepancies between the stream-flow of the model forced with test data and the observed stream-flow (this method is referred to as model error hereafter). Control data are the model forcing data used for model calibration. For the evaluation of the potential evapotranspiration records using the error propagation method, it is presumed that a reliable precipitation dataset exists and that the flow simulated using the control input data can be subsequently used to evaluate the test input

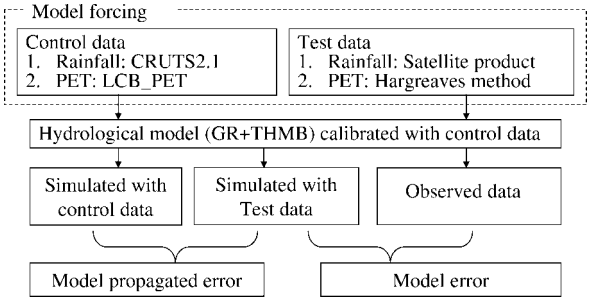

Figure 6. Methodology for the evaluation of the estimated meteorological records. LCB_PET is the time series of Penman potential evapotranspiration (PET) estimated with climate data from CRUTS2.1.

data. Both model error and model-propagated errors are expressed using NSE (Equation (4)) and the overall Volume error (Equation (5)):

$$Volume\ error = \frac{\sum_{i=1}^{n}(e_i - m_i)}{\sum_{i=1}^{n} m_i} \quad (5)$$

where e is the model estimated value, and m is the measured (control) value when model error (model propagated error) is quantified.

This approach involves: (1) the selection of control inputs, (2) the selection of flow simulation model, and (3) the calibration of parameters of the hydrological model. Since the gridded precipitation data of CRU and the LCB_PET have been used in a number of studies in the past in the LCB region, they were used as the control precipitation and potential evapotranspiration data.

3.5.2.1. Hydrological model: To evaluate the estimated meteorological records, the GR + THMB flow simulation model was used. The model includes GR2M (Makhlouf and Michel, 1994), a conceptual hydrological model for runoff production, and the Terrestrial Hydrology Model with Biochemistry (THMB) (Coe, 2000) for routing flow through rivers and lakes. The GR + THMB is a gridded model (Delclaux *et al*., 2008) that takes into account the spatial variability in climate inputs and watershed characteristics and provides information on the water fluxes at each grid cell.

The GR2M model has been widely applied for modelling flow in Western African basins (e.g. Niel *et al*., 2003; Mahé *et al*., 2005). Owing to its simplicity of application and general applicability especially in regions that are similar to the one included in these previous studies, GR2M was selected as a runoff production module. The detailed description of the GR2M model structure can be found in Makhlouf and Michel (1994). The capacity of soil water content A and a parameter $X1$, which adjusts both potential evaporation and rainfall by the same proportion by multiplying them, are the two parameters of the GR2M model. The gridded value of maximum soil water content A of GR2M was estimated from the maximum water holding capacity derived from the soil map of

FAO (Mahé *et al*., 2005). However, since the estimation of the *X1* parameter solely from land surface characteristics is difficult, it is estimated through model calibration.

Similarly, the THMB model has also been used a number of times to simulate the time-varying flow and storage of water in terrestrial hydrological systems including rivers, lakes and wetlands. THMB routes the surface run-off and subsurface runoff generated by the runoff production model GR2M to the outlets of basins or sills of lakes. The detailed description of the structure of the routing model can be found in Coe (2000). The water transport in THMB is represented by the time dependent change of three water reservoirs. The first is the river water reservoir, which contains the sum of upstream and local water in excess of what is required to fill a local water depression. The second reservoir is the surface runoff pool, which contains water that runs from the surface towards a river, and the third reservoir is the subsurface runoff pool, which contains water that flows through the local soil column that is flowing towards a river. The water entering the hydrological network is the sum of the land surface runoff, subsurface drainage, and flux of water from upstream grid cells. The solution of the governing equations of GR + THMB involves the estimation of the production parameters of GR2M and the residence time for three reservoirs. The version of the THMB model used here differs from the original THMB version (Coe, 2000) in the way the flow directions are calculated. In this study, the flow directions within topographic depressions and prescribed floodplains are dynamically calculated using water head as a controlling factor for the determination of flow direction, whereas the flow direction elsewhere within the basin is derived based on the ground elevation. The extent of floodplains (i.e. Salamat, Massenya and Yaere) within the LCB is prescribed within the model.

The gridded rainfall and potential evapotranspiration are the primary inputs to the GR + THMB model. The additional model inputs include local topography, drainage direction map, and potential water area maps. For these inputs, the datasets derived by Le Coz *et al*. (2009) were used. These datasets were derived from 3″ SRTM DEM by filtering and then resampling to 5′ DEM *via* the nearest neighbour method. In this study, owing to the computational limit and due to the unavailability of forcing data at higher resolution, the model was simulated with a $5' \times 5'$ grid size.

3.5.2.2. Model calibration: Rainfall-runoff models require the calibration of some key parameters to yield reliable predictions (Gupta *et al*., 2003). The goal of calibration is to adjust the model's parameters so that the differences between observed and simulated stream-flow values are minimal. In this study, the closeness of fit was evaluated qualitatively using visual inspection and quantitatively using the following objective criteria: (1) the NSE (Equation (4)) that reflects the overall agreement of the shape of the hydrograph, and, (2) Volume error (Equation (5)) that reflects the agreement between simulated and observed runoff volumes.

Table I. Characteristics of streamflow gauging stations used for model calibration and for evaluation of meteorological records.

S. no	Station	Area (km^2)	Lat	Lon	River system
1	Manda (Ma)	83 000	9.18	18.2	Chari
2	Sahr (Sa)	193 123	9.15	18.41	Chari
3	Bousso (Bou)	450 000	10.5	16.71	Chari
4	Bongor(Bo)	73 700	10.26	15.41	Logone
5	Ndjamena (Nd)	600 000	12.1	15.3	Chari/Logone

In this study, the Latinized Hypercube Sampling (LHS) technique was used as a tool for model calibration. The LHS technique is a constrained sampling technique where the input parameter range is divided into equi-probable non-overlapping intervals. The LHS technique can handle a wide variety of complexity such as parameter correlation and random pairing of parameter sets.

In GR + THMB, the time constants for surface and sub-surface reservoirs of THMB, which are both spatially lumped parameters over the basin, were selected from an earlier application of same model within the LCB (e.g. Coe and Foley, 2001). However, the reference velocity, a basin average parameter, and the adjustment factor *X1* of GR2M, a lumped value over sub-basins, were estimated through model calibration. The observed monthly flows from the River Chari at Sahr andi at Manda, the River Logone at Bongor and the River Chari at N'Djamena were used (Table I). The LCB_PET and CRU rainfall were used as model inputs for the calibration and validation of these parameters.

4. Results and discussion

4.1. Pairwise comparison of rainfall estimates

Figure 7 shows the overall scatter diagrams for the CRU/rain gauge, GPCP/rain gauge, TRMM/rain gauge, CRU_GPCP/rain gauge, CRU_TRMM/rain gauge, and Ave(GPCP, TRMM)/rain gauge along with the regression line and the one-to-one line. The period from 1998 to 2007 was used for all datasets except for the CRU/rain-gauge. For the CRU/rain gauge, the period from 1990 to 2002 was used because CRU is available only until 2002. On average, all six datasets were in agreement with the rain gauges. However, one apparent difference observed among the datasets was the systematic error in the satellite estimated values as compared to gauge values such as, the overestimation of low rainfall and the underestimation of high values. RFE2.0 is quantitatively more accurate (correlation coefficient $(r) = 0.9$; RMSE = 27 mm *per* month) than GPCP. However, since these data are only available after 2002, the overlapping period between RFE2.0 and the rain gauges is significantly lower than the other two satellite rainfall products. Therefore, RFE2.0 was not used

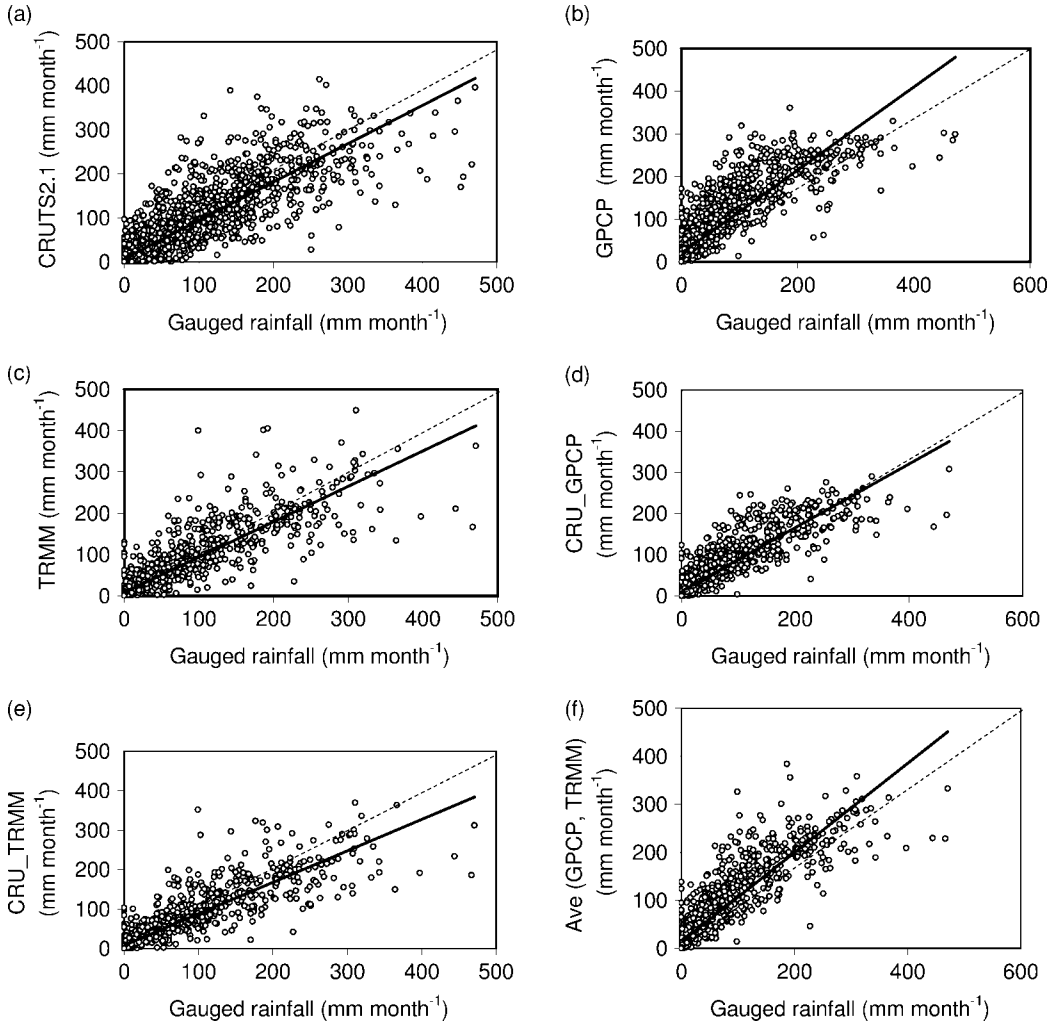

Figure 7. Scatter plot comparison between rainfall from gauges and: (a) CRUTS2.1 (1990–2002), (b) GPCP (1998–2007), (c) TRMM (1998–2007), (d) CRU_GPCP (1998–2007), (e) CRU_TRMM (1998–2007), and (f) Ave(GPCP, TRMM) (1998–2007).

for the extension of rainfall records in this study. The estimates from the CRU_GPCP and CRU_TRMM are significantly similar to the estimates from CRU. The average biases in monthly rainfall are 0.7, 19.2, 1.8, 1.04, −0.9, and 11.1 mm *per* month for CRU, GPCP, TRMM, CRU_GPCP, CRU_TRMM, and Ave (GPCP, TRMM) respectively. Since CRU, CRU_GPCP and CRU_TRMM are significantly similar, Table II only includes the results of pairwise comparisons made between rain gauges and CRU, GPCP, and TRMM.

Although CRU and satellites tend to underestimate rainfall in most stations located in the southern humid part of the basin and overestimate rainfall in the northern semi-arid part of the basin, the agreement (NSE) between gauge and satellite estimates are acceptable in most of the stations.

Table III shows the zonal average statistics estimated from pairwise comparisons. The performances of both GPCP and TRMM resulted in marginal improvements in the estimates. For GPCP, the bias in the annual average rainfall is positive (overestimation) in all three zones, whereas for CRU and TRMM it is negative in humid zones and positive in arid and semi-arid regions. Furthermore, the degree of agreement between the satellite estimates and gauge values varies among regions.

Figure 8(a) and (b) show the spatial distribution of bias for the period 1998–2002. In particular, the spatial bias for GPCP is higher than for TRMM. Both GPCP and TRMM have a propensity to underestimate the values in the north-northwest and eastern mountainous regions. A probable explanation for this underestimation in these regions is the inability of satellite algorithms to account for rainfall due to warm air. Moreover, this underestimation could also have been augmented by elevation effects that are included in interpolation algorithms of CRU estimates. In the central part of the basin, both GPCP and TRMM overestimate the CRU values (positive bias), but the overestimation by GPCP is higher than by TRMM. This overestimation can be related to the way these products are derived. First, satellite algorithms tend to overestimate rainfall in this region of Africa as mentioned by McCollum *et al*. (2000): this could be due to abundance of aerosol content in air mass and to the higher base of clouds. Second, GPCP and TRMM products use GPCC rain gauge data, which

Table II. Comparison between rainfall estimates from gridded precipitation products (CRU and satellite) and rain gauges located within Lake Chad Basin.

S. no	Station	Location		CRUTS2.1				GPCP(0.5°)				TRMM(0.5°)			
		Lat	Lon	n[a]	NSE	RMSE[b]	Bias[b]	n	NSE	RMSE[b]	Bias[b]	n	NSE	RMSE[b]	Bias[b]
1	Tesker	15.1	10.7	143	0.39	0.5	4.1	73	0.34	2.7	10.9	61	0.66	2.2	−3.1
2	N Guigmi[c]	14.3	13.1	157	0.80	0.7	−0.6	111	−0.26	3.2	18.5	99	0.17	2.9	12.5
3	Mao Meteo	14.1	15.3	129	0.68	1.4	0.7	49	0.08	6.0	20.8	37	0.37	5.5	12.2
4	Goure[c]	13.8	10.3	128	0.54	1.3	2.4	60	0.30	5.7	20.0	53	0.80	2.8	−1.8
5	Zinder[c]	13.8	9.0	144	0.83	0.4	0.8	60	0.28	5.8	24.0	60	0.81	3.0	−0.6
6	Sayam Cmi	13.7	12.5	157	0.80	0.6	1.7	73	−0.08	5.0	21.2	61	0.92	1.5	2.4
7	Goudoumaria	13.7	11.2	115	0.54	1.2	9.4	47	−0.03	8.6	34.5	41	−0.07	9.8	21.8
8	Moussoro	13.7	16.5	157	0.69	0.7	5.9	95	0.39	4.6	21.4	83	0.79	3.0	4.3
9	N Gouri	13.6	15.4	157	0.88	0.5	−2.1	110	0.29	4.3	24.2	98	0.85	2.1	0.2
10	Cheri	13.4	11.4	149	0.71	1.6	3.6	65	0.45	6.7	26.2	53	0.64	6.1	2.3
11	Maine Soroa	13.2	12.0	157	0.67	0.7	4.8	112	0.58	2.7	16.6	100	0.93	1.8	0.8
12	Chetmari	13.2	12.4	134	0.62	0.5	−1.0	62	0.43	4.6	18.4	52	0.77	1.9	3.0
13	Massaguet	12.5	15.4	71	0.71	1.0	5.6	47	−1.28	7.7	24.4	35	0.65	4.2	6.6
14	Bokoro	12.4	17.1	146	0.94	1.7	−2.7	111	0.71	3.9	18.7	103	0.70	4.2	3.5
15	N'Djamena[c]	12.1	15.0	153	0.70	1.1	5.8	73	−0.11	5.8	26.4	61	0.68	3.4	1.7
16	Kano[c]	12.1	8.5	125	0.68	2.2	−25.8	44	0.83	9.6	−16.9	32	0.50	7.0	−50.5
17	Maiduguri[c]	11.9	13.1	128	0.88	1.9	0.5	44	0.72	7.2	19.3	32	0.74	9.0	0.2
18	Dourbali	11.8	15.9	51	0.78	2.4	6.7	39	0.71	7.5	29.4	39	0.85	5.3	5.9
19	Potiskum	11.7	11.0	138	0.72	1.9	10.9	54	0.70	6.9	21.1	42	0.68	8.7	7.6
20	Bougoumene	11.5	15.4	67	0.71	3.3	10.8	49	0.66	6.9	27.6	49	0.76	5.8	12.7
21	Massenya	11.4	16.2	123	0.82	1.5	3.4	62	0.87	4.1	14.8	50	0.93	3.5	−3.6
22	Moura	10.6	14.3	143	0.78	2.7	5.4	59	0.85	5.3	6.4	47	0.82	6.5	11.2
23	Bousso meteo	10.5	16.7	143	0.88	1.6	−4.6	59	0.75	6.1	15.6	47	0.77	7.0	−10.8
24	Moundou meteo[c]	8.6	16.1	128	0.74	4.4	−2.0	46	0.47	8.1	32.7	34	0.82	16.0	−8.7
25	Moissala S/Pref	8.3	17.8	143	0.63	2.4	4.1	59	0.72	7.1	11.2	47	0.88	5.3	−0.4
26	Bossembel[c]	5.3	17.6	32	0.92	6.4	−12.0	15	0.78	16.0	−11.0	15	0.92	9.9	−20.4

[a] n is the number of months.
[b] RMSE and bias measured in mm month^{-1}.
[c] Gauging stations used in CRUTS2.1 estimates.

Table III. Statistics of zonal averages made from pair wise comparison between estimates from gridded precipitation products (CRU and satellite) and gauging stations.

S no	Statistics	Zone	CRU (0.5°)	GPCP (0.5°)	GPCP (1°)	TRMM (0.25°)	TRMM (0.5°)	CRU_GPCP	CRU_TRMM	Ave (GPCP, TRMM)
1	Zonal average NSE	Humid	0.75	0.77	0.73	0.76	0.77	0.77	0.79	0.83
		Semi arid	0.76	0.71	0.54	0.78	0.79	0.80	0.79	0.76
		Arid	0.81	0.41	0.39	0.69	0.69	0.81	0.77	0.67
2	Zonal average RMSE	Humid	52.94	52.32	56.09	54.00	53.33	53.29	51.53	46.36
		Semi arid	34.97	45.79	49.15	34.73	34.56	33.54	34.28	36.82
		Arid	23.50	40.48	41.08	30.04	29.96	23.50	25.73	30.85
3	Zonal average bias	Humid	−6.12	9.06	11.86	−9.24	−9.99	−8.83	−12.86	−0.07
		Semi arid	4.30	22.34	23.76	2.63	3.63	4.25	2.38	13.36
		Arid	1.79	20.33	19.57	4.33	4.28	1.79	0.50	12.80

overestimate CRU data in northwestern Africa (Fiedler and Doll, 2007). These combined effects probably lead to an overall overestimation of satellite estimated rainfall in the central part of the LCB with respect to the CRU data.

For both of the satellite products, the spatial RMSE decreased from the southern to northern part of the basin (Figure 8(c) and (d)). It is obvious because RMSE relates better to the estimation efficiency of extremes and because there is a strong negative gradient in the rainfall

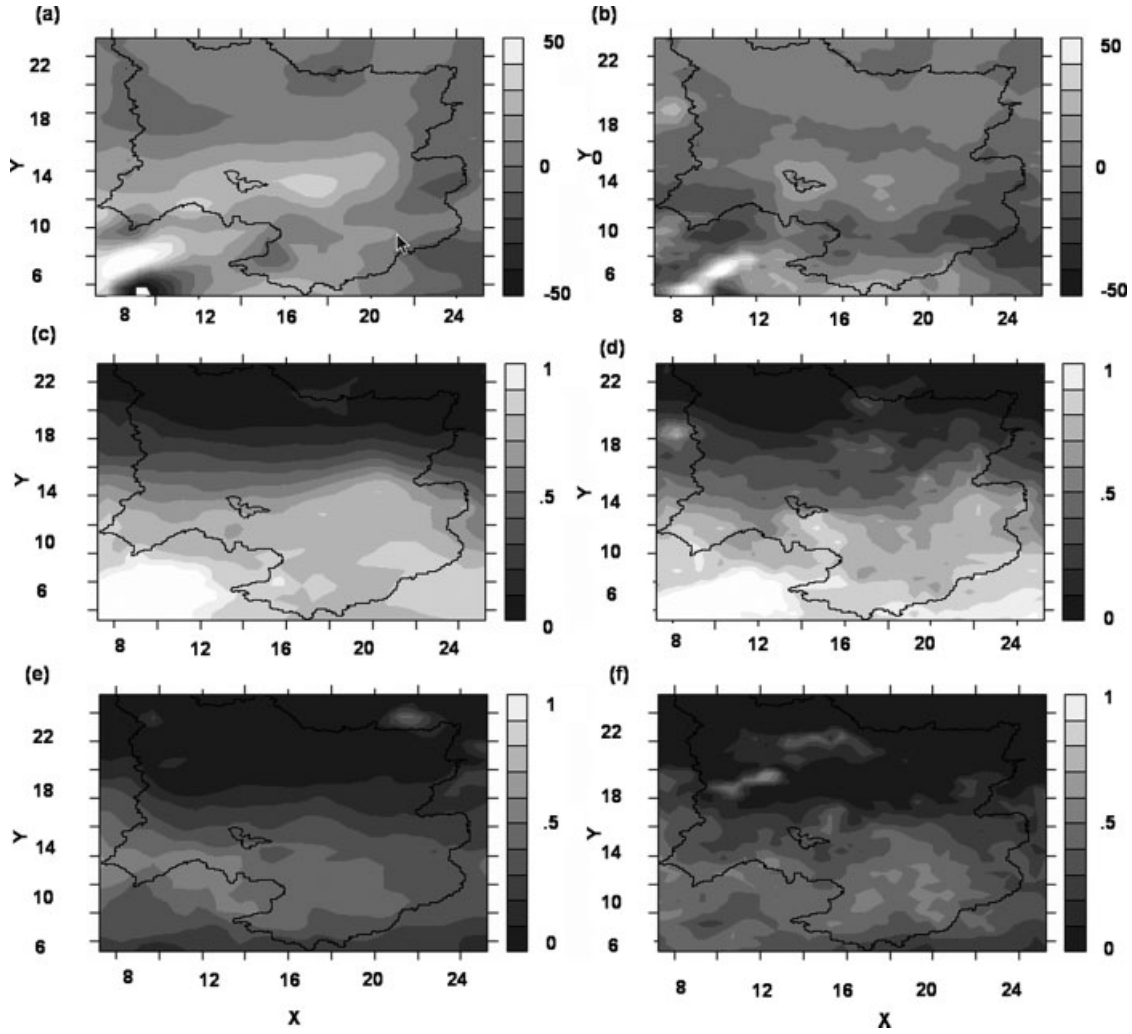

Figure 8. Comparison of spatial rainfall estimates between satellite precipitation products and CRU rainfall over the 1998–2002 period: (a) and (b) maps of bias of GPCP and TRMM with respect to CRU, (c) and (d) maps of RMSE of GPCP and TRMM with respect to CRU, and (e) and (f) maps of coefficient of determination (R2) of GPCP and TRMM with respect to CRU.

from the southern to northern part of the basin. Similarly, Figure 8(e) and (f) show the spatial distribution of R^2 measure of fitness for both GPCP and TRMM. The values of R^2 range from 0.7 to 0.9 in the southern hydrologically active regions indicating a good agreement between the two estimates from a hydrological perspective. Typically, in the centre part of the basin the R^2 corresponding to estimates from GPCP is higher than from TRMM.

4.2. Pairwise comparison of PET estimates

Table IV shows the predictive performance of the calibrated constants and constants adopted from the literature. For both periods, i.e. the calibration and validation period, the coefficient recalibrated from NCEP/NCAR resulted in minimum bias and RMSE compared to the coefficients adopted from the literature. Figure 9 shows the scatter plot between measured PET values and those calculated using the Hargreaves method for the period from 1965 to 1972, including both original and recalibrated constants from NCEP/NCAR data. It is apparent that the bias in the estimated PET, with respect to measured PET is higher using constants from the literature than with constants recalibrated from NCEP/NCAR reanalysis datasets. Therefore, the latter were used to construct the gridded PET data until 2007 for the LCB region.

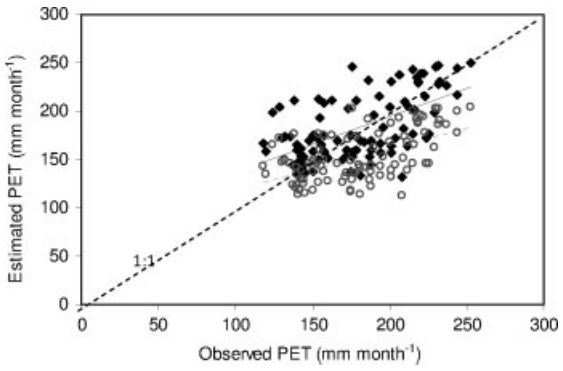

Figure 9. Scatter plot comparison between observed and Hargreaves estimated potential evapotranspiration for the evaluation period 1965–1972. Recalibrated (NCEP/NCAR) (◆), Literature (○), Linear (Recalibrated (NCEP/NCAR)) (———), Linear (Literature) (- - - - - -).

Table IV. Performance of Hargreaves potential evapotranspiration for two different sets of coefficients.

S no	Scheme	Period	Hargreaves method					
			Parameter		Performance			Input data
			a	*b*	Correlation	RMSE (mm month^{-1})	Bias (mm month^{-1})	
1	Literature	Calibration: 1973–1977 Validation: (1965–1972)	0.015	18	0.72 (0.55)	33.23 (39.5)	22.6 (26.9)	Temperature and solar radiation from NCEP/NCAR
2	GCM	Calibration: 1973–1977 Validation: (1965–1972)	0.022	8	0.73 (0.58)	26.44 (30.9)	8.14 (2.5)	

Hargreaves method is forced with same input datasets from NCEP/NCAR reanalysis for all coefficients.

The spatial distributions of RMSE and bias in climatological PET estimates (1960–1990) and FAO gridded Climatological values (1960–1990) are shown in Figure 10(a) and (b). The climatological output from the Hargreaves method underestimates the PET of FAO in the northern part of the basin, and overestimates it in the southern part. However, in the central part where Lake Chad is situated, the bias estimation is low. Similarly, Figure 10(c) and (d) show the spatial value of RMSE and bias calculated from the time series of the Hargreaves PET and the LCB_PET (1960–1975). It shows that within the Chari-Logone basin, the Hargreaves method overestimates PET in the range of 0–20 mm *per* month, but in the northern part it underestimates PET. Regarding RMSE, it varies from 10 to 20 mm *per* month within the Chari-Logone basin. These discrepancies can be attributed to the use of solar radiation data from NCEP/NCAR and the calibration dataset used for the estimation of the constants. The solar data are completely a product of a model and are highly dependent on the GCM parameterization and the calibrated constants that were derived from measurements in the Bol Matafo station, is located in a more arid area as compared to the southern part of the basin.

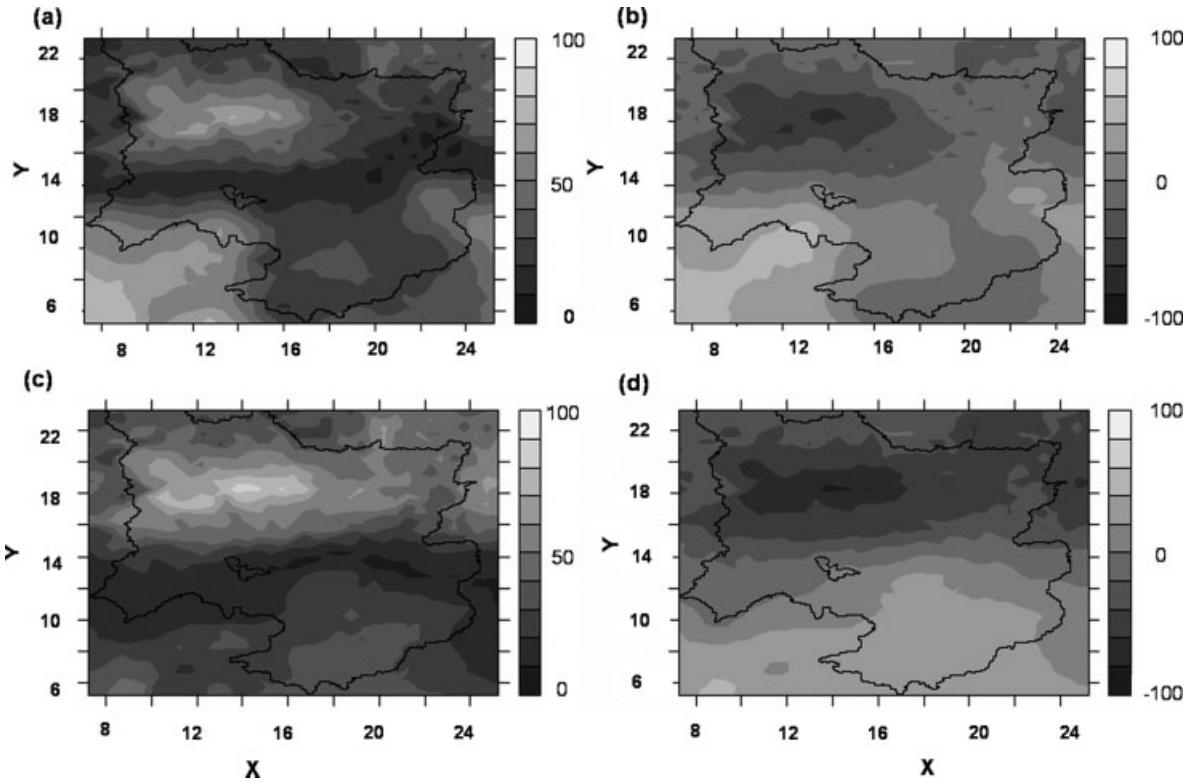

Figure 10. Comparison of spatial potential evapotranspiration estimates between Hargreaves PET and Penman PET and climatological FAO PET: (a) and (b) maps of RMSE and bias of Hargreaves PET with respect to FAO PET over the 1960–1990 period, (c) and (d) maps of RMSE and bias of Hargreaves PET with respect to Penman PET over 1960–1975.

4.3. Error propagation through hydrological models

The hydrological model was calibrated for the period of 15 years, from 1960 to 1975. Since the annual variation of precipitation during the 1940–1990 period showed a considerable decreasing trend, especially after 1970, the period of 1960–1975 was chosen for model calibration because this period represents both wet and dry climates within the basin. Figure 11 shows that the simulated flow at two gauging stations, N'Djamena on the River Chari and Bongor on the River Logone, explains much of the variability in these observations. The NSE and overall volume errors for the simulated flow of the River Chari at N'Djamena were 0.87 and −7%, respectively. Similarly, for the River Logone at Bongor, the NSE and volume errors were 0.85 and 9%, respectively. For the validation period (1998–2002), the NSE and volume errors in annual runoff of the River Chari at N'Djamena were 0.82 and −20%, respectively.

This model apparently underestimated the flow during the validation period, even though the spatial average precipitation over the basin decreased by nearly 12% compared to the calibration period. Therefore, the underestimation of flow in the validation period (1998–2002) is more likely to be associated with differences in the spatial and temporal characteristics of the zone. For the evaluation of two key meteorological records, a single set of model parameters that corresponds to the best simulation in all internal gauging stations was used, since discussions on parameter uncertainty is beyond the scope of this study.

4.3.1. Rainfall estimates

Figure 12(a) and (b) show the spatial average rainfall derived from the precipitation datasets over two sub-basins, N'Djamena and Bongor. Over these sub-basins, the spatial average values from satellite-based products are significantly similar (at 5% significant level) with the estimates from CRU. Figure 12(c) and (d) show the simulated flows at two gauging stations, N'Djamena and Bongor, when the model is applied with the data from CRU, TRMM, GPCP, and Ave(GPCP, TRMM). Since the average rainfall in the basin and the flow simulated by

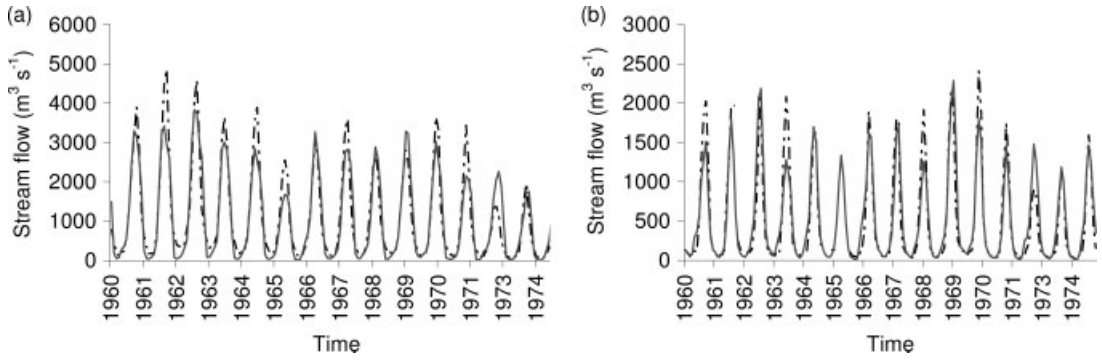

Figure 11. Observed and simulated flows at N'Djamena and Bongor stations over the calibration period (1960–1975). Obs (- - -), Sim (——).

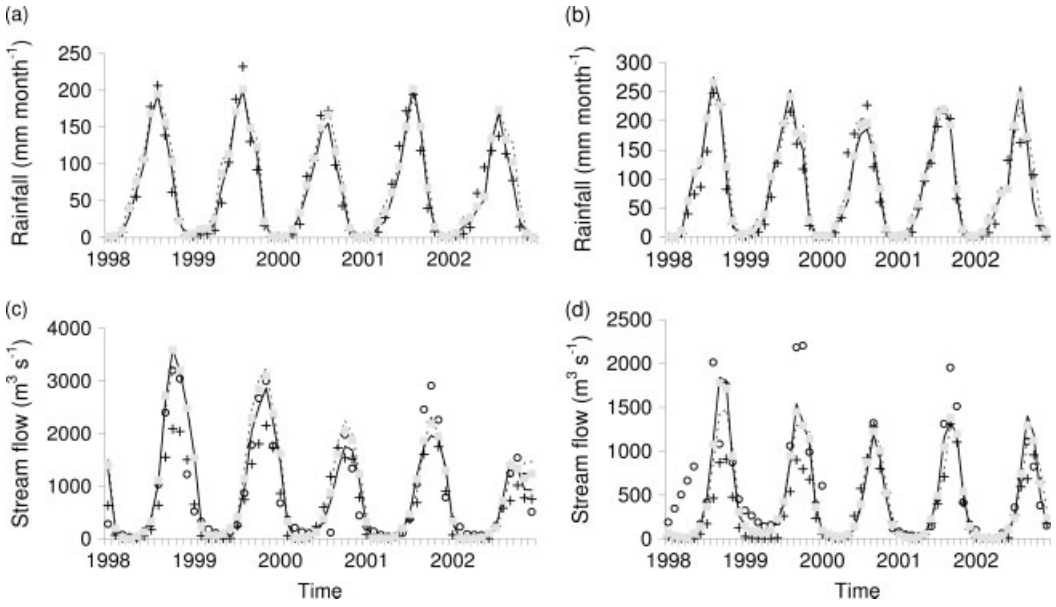

Figure 12. (a) and (b) Spatial average rainfalls over Chari and Logone sub-basin at N'Djamena and Bongor of Lake Chad Basin and (c) and (d) Simulated flow at N'Djamena and Bongor gauging stations. The model is forced with rainfall estimates from CRU, TRMM, GPCP and Ave (GPCP, TRMM). CRU (+), TRMM (——), GPCP (- - -), Ave (○), Obs (flow) (⊙).

CRU_GPCP and CRU_TRMM are both similar to CRU rainfall and the flow simulated by CRU, they are not included in Figure 12.

Figure 13 shows the performance of GR + THMB in four sub-basins, when different rainfall datasets are applied in two-dimensional objective space (NSE, Volume error). These performances were measured with respect to the simulated control output (Figure 6). Each point in this figure represents the model's performance for NSE and volume error at a specified gauging location and for a specified input dataset. To quantify the model propagated error objectively, the average Euclidean distance of each point was determined from the ideal performance point (i.e. NSE = 1, and volume error = 0). These values are 1.73, 1.17, 0.57, 0.4, and 1.21 for GPCP, TRMM, CRU_GPCP, CRU_TRMM, and Ave(GPCP, TRMM), respectively. These results indicate that the model propagated errors are smaller for CRU_GPCP and CRU_TRMM as compared to GPCP, TRMM, and Ave(GPCP, TRMM), which is not surprising because these datasets were prepared by concatenating CRU and estimates were inferred from the linear relationship between GPCP and CRU during an overlapping period.

Figure 14 shows the bias in the spatial average value of satellite rainfall with respect to CRU and the consequent bias in the stream flow. Compared to CRU, GPCP overestimates spatial average rainfall by nearly 15% in all sub-basins. Alternatively, the bias in the spatial average rainfall for TRMM is lower than for GPCP. For TRMM, the bias varies from −3 to 10% among sub-basins. TRMM underestimates the values over the Sahr sub-basin, but

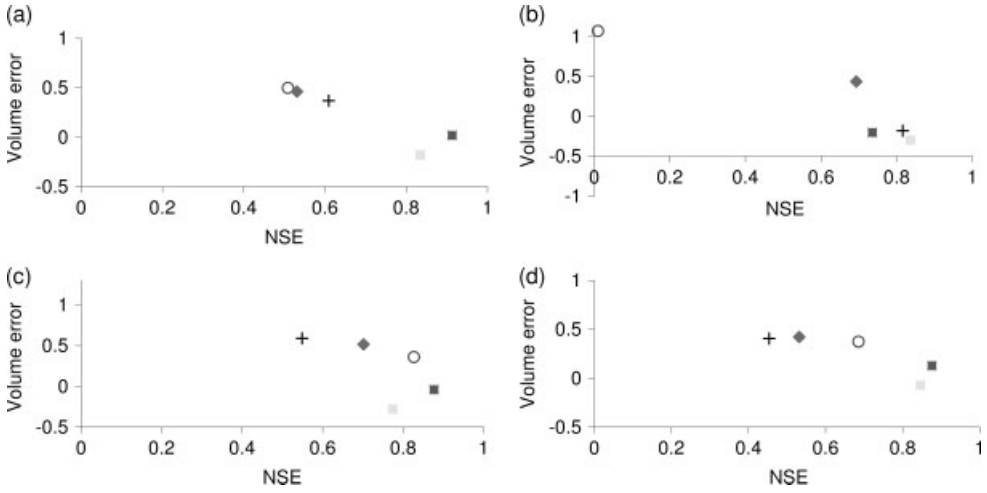

Figure 13. Performances of model forced with rainfall estimates from satellite products measured with respect to flow simulated by CRU rainfall over 1998–2002 (i.e., Satellite-CRU common period). Performances are shown in the model's objective space (Nash Sutcliffe Efficiency NSE, Volume error) for (a) N'Djamena, (b) Sahr, (c) Manda and (d) Bongor. GPCP (○), GPCP_CRU (■), TRMM (+), TRMM_CRU (□), Ave (◆).

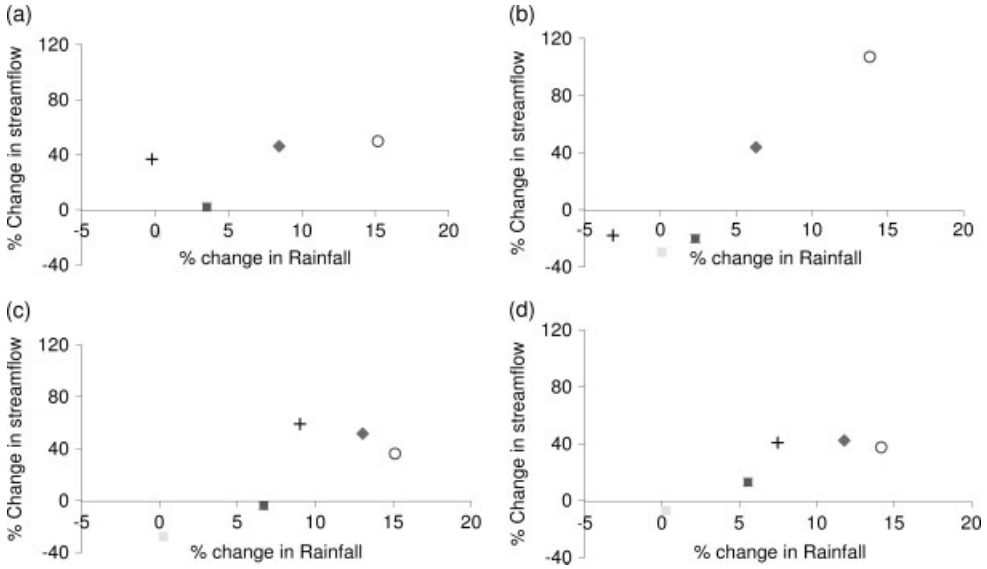

Figure 14. Volume error in average rainfall from satellite products with respect to CRU and consequent Volume error in simulated flow with respect to flow simulated by CRU over 1998–2002 for (a) N'Djamena, (b) Sahr, (c) Manda and (d) Bongor. GPCP (○), TRMM_CRU (□), TRMM (+), GPCP_CRU (■), Ave (◆).

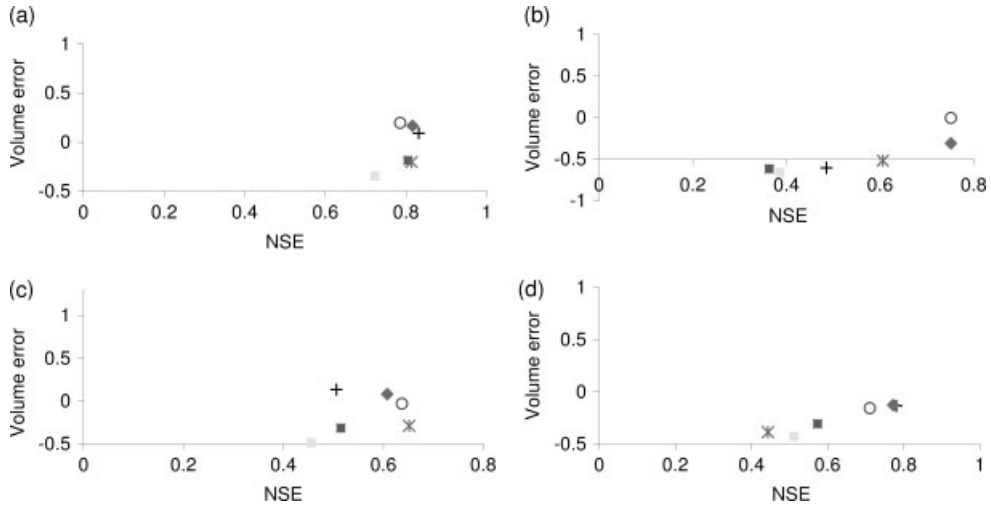

Figure 15. Performances of model forced with rainfall estimates from satellite products measured with respect to observed flow over the 1998–2002 period. Performances are shown in the model's objective space (Nash Sutcliffe Efficiency NSE, Volume error) for (a) N'Djamena, (b) Sahr, (c) Manda and (d) Bongor. CRU (✳), GPCP_CRU (■), GPCP (○), TRMM_CRU (□), TRMM (+), Ave (◆).

overestimates over the Bongor sub-basin. This discrepancy between TRMM and GPCP can be attributed to differences in the rainfall processes accounted for by respective satellite algorithms and error models implemented to merge various types of information and spatial resolutions. Furthermore, it is also evident that the reductions in runoff are proportionately greater than reductions in rainfall. For GPCP, TRMM, and Ave(GPCP, TRMM), the percentage changes in rainfall are typically amplified four times in the runoff in most of the sub-basins, except the Sarh. At the Sarh sub-basin, both GPCP and TRMM result in much larger amplification (nearly by a factor of seven) in changes in runoff for similar changes in rainfall. The Sarh sub-basin houses immense wetlands, the Salamat wetlands, and contains numerous endorheic depressions. These land surface characteristics make the basin's response more sensitive and more nonlinear to rainfall estimates. In particular, the annual average runoff coefficients for the Sahr sub-basin (5%) are markedly lower than the Manda (15–20%) and Bongor (20%) regions. Such nonlinear behaviour is common in basins that have low runoff coefficients (e.g. Nemec and Schaake, 1982). These data further highlight the necessity of reliable estimations of precipitation in such basins. Surprisingly, the comparison of the performances of the model runoff with rainfall scenarios, as defined in Section 3.3, against the observed stream-flow data reveals that TRMM rainfall results in improved simulation in flow at the N'Djamena and Bongor stations compared to CRU and GPCP. However, GPCP performed better at Manda and Sahr (Figure 15) than TRMM and CRU. Similarly, the average Euclidean distance of each point from the ideal performance point was calculated to quantify the model error. These value are 1.07, 0.62, 0.99, 1.21, 1.40 and 0.66 for CRU, GPCP, TRMM, CRU_GPCP, CRU_TRMM and Ave(GPCP, TRMM), respectively. They indicate that model errors are less for GPCP, TRMM and Ave(GPCP, TRMM) as compared to CRU, CRU_GPCP< and CRU_TRMM. In this context, extension of rainfall records using satellite imagery is appealing from a hydrological modelling point of view. Furthermore, since GPCP and TRMM tend to perform differently among basins and since the amplification of bias in rainfall into runoff is markedly different among the basins, the possibility of combining different sources of datasets for simulation modelling of the LCB is plausible.

4.3.2. *PET estimates*

Figure 16(a) shows the performances of GR + THMB measured with respect to the control simulation (1960–1975) for each sub-basin when the model is forced with the Hargreaves PET. Since both the NSE and volume error are close to 1 and 0 respectively, the Hargreaves PET and the LCB_PET are similar from a hydrological model's prospective. Figure 16(b) shows the bias in the Hargreaves PET with respect to the LCB_PET and consequent bias in the simulated stream-flow. The marginal amplification in the change in stream-flow resulting from the change in PET is observed at all gauging stations. For example, an average decrease in 1% of PET results in nearly a 2% increase in the stream-flow at N'Djamena. However, Sahr and Bousso sub-basins are particularly sensitive to PET estimates compared to Bongor and Manda. At Sahr and Bousso, underestimations of 1% by PET results in nearly a 7% increase in runoff.

Regarding the model's error, the performances of the model in the objective space shown in Figure 17 reveals no significant detrimental effect. For each station, the points corresponding to model performance obtained with the two PET datasets are apparently similar. This is particularly true for the N'Djamena station indicating that at the whole basin scale, the Hargreaves PET and the LCB_PET are indistinguishable from the hydrological point of view.

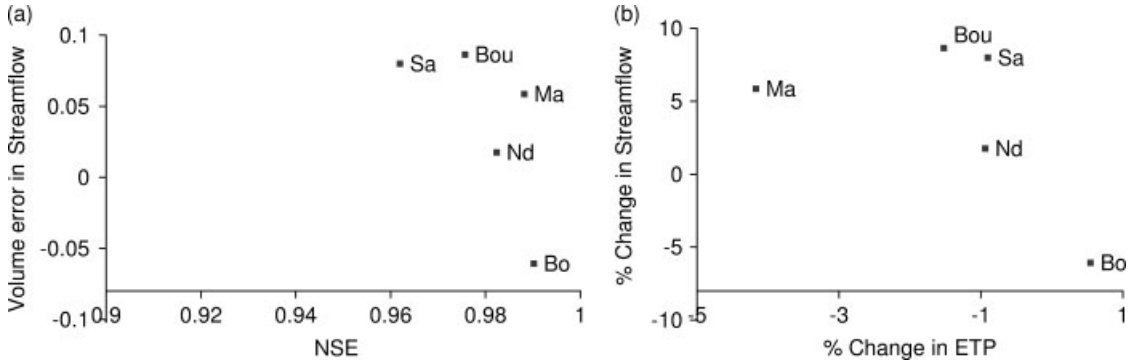

Figure 16. (a) Performance of model forced with Hargreaves potential evapotranspiration (PET) measured against the flow simulated by control PET dataset (i.e., LCB_PET) over 1960–1975, (b) Volume error in Hargreaves PET and Penman PET (LCB_PET) and consequent Volume error in the simulated flow in five gauging stations (labels Ma, Sh, Bou, Bo and Nd correspond to the stations located at Manda, Sahr, Bousso, Bongor and N'Djamena).

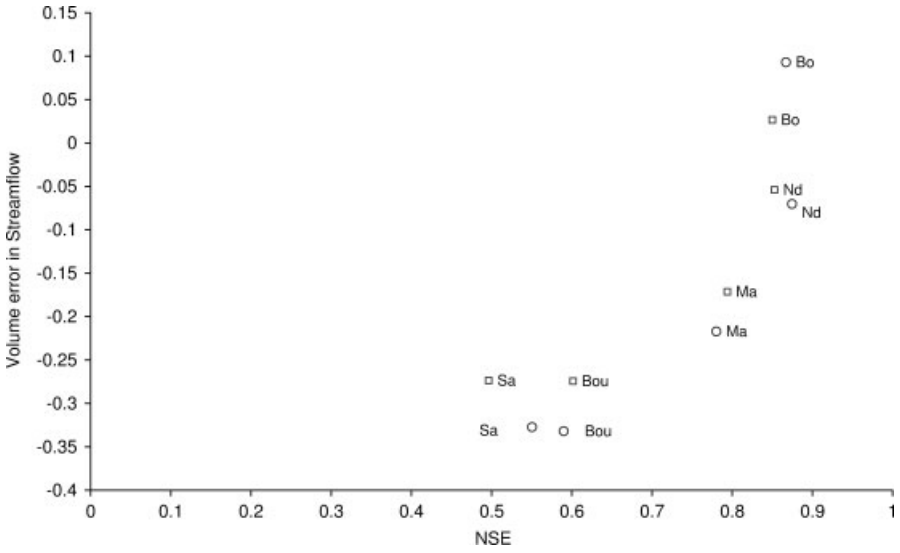

Figure 17. Performances of flow simulated by the model forced with Hargreaves estimated potential evapotranspiration (PET) and Penman PET (LCB_PET) against observed flow in five gauging stations (labels Ma, Sh, Bou, Bo and Nd correspond to the stations located at Manda, Sahr, Bousso, Bongor and N'Djamena). Hargreaves estimate (□), Ctl PET (○).

5. Conclusions

Estimation of reliable rainfall data for the hydrological modelling of the Lake Chad Basin over the present decade poses a hindrance to the use and evaluation of a wide range of new and relevant hydrological information that can be extracted from satellite altimetry, gravitometry and imagery. This is mainly due to sparse distribution of gauging stations and difficulty in assessing the data. Although satellite rainfall datasets have the potential to overcome these constraints, they have their own limitations in terms of accuracy, space-time resolutions and data time length. Hence, their utility for hydrological applications needs to be assessed.

Pairwise comparisons between measured rainfall at stations and satellite-derived rainfall showed that satellite-derived values tend to overestimate low values and underestimate high values. Both GPCP and TRMM showed the propensity to underestimate (overestimated) the values with respect to CRU estimates in the mountainous (central) region. Subsequently, satellite products were evaluated using the GR + THMB hydrological model. Three satellite-derived rainfall values, i.e. GPCP, TRMM and Ave(GPCP, TRMM), showed the tendency to overestimate flows in the sub-basins of the LCB. The differences in the volume of rainfall with respect to CRU rainfall are typically amplified (positively) by a factor ranging from four to seven into the simulated runoff. Such variation in the amplification of a model's response among sub-basins stresses the need for a more reliable spatial estimate of precipitation. Comparison of the satellite rainfall simulated flows with observed flow shows that the satellite products result in better model performance than CRU.

Regarding the potential evapotranspiration (PET), the Hargreaves PET is in good agreement with the time series of PET estimated using the Penman method and with climatological values from the FAO dataset, particularly in the southern part of the basin. However, they perform poorly in northern and eastern parts of the

basin. The model appears less sensitive to differences in the Hargreaves PET and Penman PET than differences in satellite rainfall and CRU rainfall. However, the increase in the simulated runoff is proportionately greater than the reduction in estimated PET. This is likely due to the presence of large wetlands that provide more opportunities for evaporation and consequently, reduced runoff.

In the framework of hydrological modelling of the LCB, this study demonstrates the usefulness of rainfall extracted from satellite products, and PET estimated from empirical methods forced with air temperature and solar radiation from NCEP/NCAR reanalysis. In particular, scenarios based on the average of TRMM and GPCP rainfall, and PET estimated from the Hargreaves method with meteorological variables from reanalysis will be used for further studies in the LCB, including floodplain dynamics assessments and evaluations of new satellite information.

List of acronyms

GPCP1DD
CRU: Climate Research Unit
FAO: Food and Agriculture Organization
GPCP: The Global Precipitation Climatology Center
GPCP1DD: Global Precipitation Climatology Project One Degree Day
LCB: Lake Chad Basin
NCAR: National Center for Atmospheric Research
NCEP: National Centers for Environmental Prediction
NSE: Nash Sutcliffe Efficiency criteria
PET: Potential Evapotranspiration
THMB: Terrestrial Hydrology Model with Biochemistry
TRMM: Tropical Rainfall Measuring Mission

Acknowledgements

This work received support from the French National Research Agency (ANR) under the Projects SAHELP and GHYRAF and from the research unit HydroSciences Montpellier. We express our gratitude to Nathalie Rouché (IRD) and Nadji Tellro Wai (DREM, N'Djamena) for their support in preparation. We also thank Gil Mahé, for his suggestions and comments. The quality of this paper has been greatly improved by the thoughtful comments from two anonymous reviewers and the Journal Editor.

References

Abtew W. 2001. Evaporation estimation for Lake Okeechobee in South Florida. *Journal of Irrigation and Drainage Engineering* **127**: 140–147.

Adeyewa DZ, Nakamura K. 2003. Validation of TRMM radar rainfall data over major climatic regions in africa. *American Meteorological Society* **42**: 331–347.

Adler RF, Huffman GJ, Chang A, Ferraro R, Xie P, Janowiak J. 2003. The version-2 global precipitation climatology project (GPCP) monthly precipitation analysis. *Journal of Hydrometeorology* **4**(6): 1147–1166.

Ali A, Amani A, Diedhiou A, Lebel T. 2005. Rainfall estimation in the sahel. Part 2: evaluation of raingauge networks in the CILSS countries and objective inter comparison of rainfall products. *Journal of Applied Meteorology* **44**: 1707–1722.

Andreassian V, Perrin C, Michel C. 2004. Impact of imperfect potential evapotranspiration knowledge on the efficiency and parameters of watershed models. *Journal of Hydrology* **286**: 19–35.

Boyer J, Dieulin C, Rouche N, Cres A, Servat E, Paturel J. 2006. *SIEREM: An Environmental Information System for Water Resources*, Vol. IAHS Publication 308. IAHS Press: Wallingford, United Kingdom.

Coe MT. 2000. Modeling terrestrial hydrological systems at the continental scale: testing the accuracy of an atmospheric GCM. *Journal of Climate* **13**: 686–704.

Coe MT, Birkett CM. 2004. Calculation of river discharge and prediction of lake height from satellite radar altimetry: example for the Lake Chad Basin. *Water Resource Research* **40**: 1–11.

Coe MT, Foley FA. 2001. Human and natural impacts on the water resources of the Lake Chad Basin. *Journal of Geophysical Research* **106**(D4): 3349–3356.

CPC. 2006. RFE2.0 rainfall estimates. [Updated 22 January 2006]. http://www.cpc.ncep.noaa.gov/products/fews/data.html#rfe2 (Accessed 1 September 2008).

Deichmann U, Eklundh L. 1991. *Global Digital Datasets for Land Degradation Studies: A GIS Approach*, *GRID Case Study Series 4*. Global Resource Information Database, United Nations Environment Programme: Nairobi, Kenya.

Delclaux F, Lecoz M, Coe M, Favreau G, Ngounou NB. 2008. Confronting models with observations for evaluating hydrological change in the lake chad basin, Africa. *13th IWRA World Water Congress*, Montpelier, VT.

Dinku T, Connor SJ, Ceccato P, Ropelewski CF. 2008. Comparison of global gridded precipitation products over a mountainous region of Africa. *International Journal of Climatology* **28**: 1627–1638.

Döll P, Kaspar F, Lehner B. 2003. A global hydrological model for deriving water availability indicators: model tuning and validation. *Journal of Hydrology* **270**: 105–134.

FAO. 2004. *Global Map of Monthly Reference Evapotranspiration – 10 Arc Minutes*, FAO: Rome, Italy.

Fiedler D, Doll P. 2007. Global modelling of continental water storage changes – sensitivity to different climate data sets. *Advances in Geosciences* **11**: 63–68.

Frappart F, Minh DK, L'Hermitte J, Cazenave A, Ramillien G, Le Toan T, Mognard-Campbell N. 2006. Water volume change in the lower Mekong from satellite altimetry and imagery data. *Geophysical Journal International* **167**: 570–584.

Gac JY. 1980. Géochimie du bassin du lac Tchad (Geochemistry of Lake Chad basin), Thèse de Doctorat d'Etat, Travaux et Documents de l'ORSTOM, ORSTOM (Office de la Recherche Scientifique et Technique d'Outre-Mer) editions, Paris, France.

GES DISC. 2010. TRMM and other sources rainfall product. [Updated August 2010]. http://gcmd.nasa.gov/records/GCMD_GES_DISC_TRMM_PR-TMI-VIRS-OTHER_3B43_V6.html (Accessed 1 September 2008).

Güntner A, Stuck J, Werth S, Döll P, Verzano K, Merz B. 2007. A global analysis of temporal and spatial variations in continental water storage. *Water Resource Research* **43**: W05416 DOI: 10.1029/2006WR005247.

Gupta H, Beven K, Wagener T. 2003. In *Model Calibration and Uncertainty Estimation*, Anderson MG (ed.). John Wiley and Sons: Chichester, United Kingdom.

Haas E, Bartholome E, Combal B. 2009. Time series analysis of optical remote sensing data for the mapping of temporary surface water bodies in sub-Saharan western Africa. *Journal of Hydrology* **370**(1–4): 52–63.

Hargreaves GH, Samani ZA. 1985. Reference crop evapotranspiration from temperature. *Transaction of the ASAE* **28**(1): 96–99.

Huffman GJ, Adler RF, Arkin P, Chang A, Ferraro R, Gruber A. 1997. The global Precipitation Climatology Project (GPCP) combined precipitation data set. *Bulletin of the American Meteorological Society* **78**: 5–20.

Huffman GJ, Adler RF, Morrissey MM, Curtis S, Joyce RJ, McGavock B. 2001. Global precipitation at one degree daily resolution from multi-satellite observations. *Journal of Hydrometeorology* **2**: 36–50.

Huffman JG, Bolvin TD. 2009. GPCP one-degree daily precipitation data set documentation. [Updated 6 July 2009]. http://www1.ncdc.noaa.gov/pub/data/gpcp/1dd-v1.1/ (Accessed 1 September 2008).

Kay AL, Davies HN. 2008. Calculating potential evaporation from climate model data: a source of uncertainty for hydrological climate change impacts. *Journal of Hydrology* **358**(3–4): 221–239.

Kuczera G, Mroczkowski M. 1998. Assessment of Hydrologic parameter uncertainty and the worth of multi-response data. *Water Resource Research* **34**(6): 1481–1490.

Le Coz M, Delclaux F, Genthon P, Favreau G. 2009. Assessment of Digital Model (DEM) aggregation methods for hydrological modeling: Lake Chad basin, Africa. *Computer and Geosciences* **35**(8): 1661–1670.

McCollum JR, Gruber A, Ba B. 2000. Discrepancy between gauges and satellite estimates of rainfall in equatorial africa. *Journal of Applied Meteorology* **39**(5): 666–679.

Mahé G, L'Hote Y, Olivry JC, Wotling G. 2001. Trends and discontinuities in regional rainfall of west and central africa: 1950–1989. *Hydrological Science Journal* **46**(2): 211–226.

Mahé G, Paturel JE, Servat E, Conway D, Dezetter A. 2005. The impact of land use change on soil water holding capacity and river flow modelling in the Nakambe River, Burkina-Faso. *Journal of Hydrology* **300**: 33–43.

Makhlouf Z, Michel C. 1994. A two parameter monthly water balance model for French watersheds. *Journal of Hydrology* **162**: 299–318.

Makkink GF. 1957. Testing the penman formula by means of lysimeters. *Journal of the Institute of Water Engineers* **11**: 277–288.

Mitchell TD, Jones PD. 2005. An improved method of constructing a database of monthly climate observations and associated high-resolution grids. *International Journal of Climatology* **25**: 693–712.

Nandakumar N, Mein RG. 1997. Uncertainty in rainfall-runoff model simulations and the implications for predicting the hydrologic effects of land use change. *Journal of Hydrology* **192**: 211–232.

Nemec J, Schaake J. 1982. Sensitivity of water resource systems to climate variation. *Hydrological Science Journal* **27**(3): 327–343.

Niel H, Paturel JE, Servat E. 2003. Study of parameter stability of a lumped hydrologic model in a context of climate variability. *Journal of Hydrology* **278**: 213–230.

Olivry JC, Chouret A, Vuillaume G, Lemoalle J, Bricquet JP. 1996. *Hydrologie du Lac Tchad (Lake Chad hydrology). Monographie hydrologique 12*. ORSTOM (Office de la Recherche Scientifique et Technique d'Outre-Mer) editions: Paris, 259.

Oudin L, Hervieu F, Michel C, Perrin C, Andreassian V, Anctil F, Loumagne C. 2005. Which potential evapotranspiration input for a lumped rainfall-runoff model?: part 2- Towards a simple and efficient potential evapotranspiration model for rainfall-runoff modelling. *Journal of Hydrology* **303**(1–4): 290–306.

Paturel J, Servat E, Vassiliadis A. 1995. Sensitivity of conceptual rainfall-runoff algorithms to errors in input data. Case study of GR2M model. *Journal of Hydrology* **168**: 111–125.

Peixoto JP, Oort AH. 1992. *Physics of Climate*. American Institute of Physics: New York, NY.

Penman HL. 1948. Natural evaporation from open water, barre soil and grass. *Proceedings of the Royal Society of London* **193**: 120–145.

Roche MA. 1980. Tracage naturel salin et isotopique des eaux du systeme du Lac Tchad (Environmental saline and isotopic tracing of Lake Chad hydrosystem), Thèse de Doctorat d'Etat, Travaux et Documents de l'ORSTOM, ORSTOM (Office de la Recherche Scientifique et Technique d'Outre-Mer) editions, Paris.

Rudolf B, Schneider U. 2004. Calculation of gridded precipitation. *Proceedings of the 2nd Workshop of the International Precipitation Working Group IPWG*, Monterey.

Sage. 2010. THMB (Terrestrial Hydrology Model with Biogeochemistry) – formerly HYDRA. [Updated 6 September 2010]. http://www.sage.wisc.edu/download/HYDRA/hydra.html (Accessed 1 September 2008).

Shahin M. 2002. In *Hydrology and Water Resources of Africa*, Singh VP (ed.). Kulwer Academic Publishers: Dordrecht, The Netherlands.

Singh VP, Xu CY. 1997. Evaluation and generalization of 13 equations for determining free water evaporation. *Hydrological Processes* **11**: 311–323.

Vörösmarty CJ, Federer CA, Schloss AL. 1998. Potential evaporation functions compared on US watersheds: possible implications for global-scale water balance and terrestrial ecosystem modelling. *Journal of Hydrology* **207**: 147–169.

Xu CY, Singh VP. 2000. Evaluation and generalization of radiation based methods for calculating evaporation. *Hydrological Processes* **14**: 339–3349.

